Intrinsic electrostatic effects in nanostructured ceramics

P. Nerikar,[1] C. R. Stanek,[1] S. R. Phillpot,[2] S. B. Sinnott,[2] and B. P. Uberuaga[1,*]
[1]*Materials Science and Technology Division, Los Alamos National Laboratory, Los Alamos, New Mexico 87545, USA*
[2]*Department of Materials Science and Engineering, University of Florida, Gainesville, Florida 32611, USA*
(Received 13 October 2009; published 23 February 2010)

Using atomic-level calculations with empirical potentials, we have found that electrostatic dipoles can be created at grain boundaries formed from nonpolar surfaces of fluorite-structured materials. In particular, the $\Sigma5(310)/[001]$ symmetric tilt grain boundary reconstructs to break the symmetry in the atomic structure at the boundary, forming the dipole. This dipole results in an abrupt change in electrostatic potential across the boundary. In multilayered ceramics composed of stacks of grain boundaries, the change in electrostatic potential at the boundary results in profound electrostatic effects within the crystalline layers, the nature of which depends on the electrical boundary conditions. For open-circuit boundary conditions, layers with either high or low electrostatic potential are formed. By contrast, for short-circuit boundary conditions, electric fields can be created within each layer, the strength of which then depend on the thickness of the layers. These electrostatic effects have important consequences for the behavior of defects and dopants within these materials.

DOI: 10.1103/PhysRevB.81.064111 PACS number(s): 61.72.Mm, 81.05.Je, 41.20.Cv

I. INTRODUCTION

As the dimensions of materials approach the nanometer scale, many new and useful properties emerge. These include enhanced radiation tolerance such as seen in CuNb multilayers,[1] superelasticity of nanostructured metals,[2] and the unique properties of ferroelectrics with nanostructured domains that are used as transducers.[3] In these and innumerable other examples, unique properties result precisely because the material has characteristic length scales on the order of nanometers. In this paper, we describe another inherently nanoscale phenomenon, in which nanostructured insulating ceramics exhibit intrinsic electric fields which do not exist in ceramics with larger characteristic dimensions. These electric fields arise from a breaking of the symmetry of the atomic structure at grain boundaries, leading to a polarity—a structural and electrostatic orientation—associated with the grain boundary and the imposition of short-circuit electrical boundary conditions that impose zero potential change across the system. By controlling the sequence of grain-boundary polarities within a layered ceramic and the electrical boundary conditions, regions of high or low potential and/or electric fields can be created in a controlled manner. This control of the electrostatics of the system may have important implications for the manipulation of the behavior of charged defects and dopants in the material.

The existence of electrostatic effects in insulating ceramics is well established. Perhaps the most widely studied electrostatic effect is that of space charge. Due to differences in the formation energy of defects, dopants, and impurities, they segregate unequally to grain boundaries or other microstructural features, giving rise to a space charge.[4,5] This leads to electric fields within the material that can play a determining role in its properties by modifying the formation energy of other dopants and defects at the boundary, and thereby influencing further segregation until a stable distribution of species is achieved.[6] Space charge involves species segregation; as such, it is a result of defect interactions with the boundary and is not inherent to the atomic structure of the boundary itself.

Duffy and Tasker[7] showed that when grain boundaries are created from polar surfaces, a dipole may be created if the spacing at the boundary is different than in the bulk region. This dipole leads to a drop in the electrostatic potential across the boundary. Further, it has been demonstrated that dipoles can be created at asymmetric grain boundaries.[8] In this paper, using atomistic simulation methods, we find that a similar effect can occur more generally, including for symmetric interfaces created from nonpolar surfaces. The direction of this potential change, related to the structural orientation—or polarity—of the boundary, can be controlled. Furthermore, by exploiting this effect, one can, at least, in principle, engineer multilayer systems in which the electrostatic potential varies from layer to layer in a defined manner that will directly influence dopant properties. Finally, by short circuiting the electrostatic potential, a long-range macroscopic, and potentially experimentally observable, electric field is created.

We illustrate this effect by examining the structure and properties of four fluorite-structured ceramic superlattices with layer thicknesses between 2 and 22 nm. The superlattice layers are delineated by $\Sigma5(310)/[001]$ symmetric tilt grain boundaries, which are chosen both because they are model boundaries and because they have been previously observed experimentally in fluorite-related materials.[9] We examine the electrostatic properties of these materials using both empirical potentials and density-functional theory (DFT).

II. METHODOLOGY

Empirical potentials are used to examine the structure and properties of layered fluorite-structure ceramics with layer spacings between 2 and 22 nm. The potentials are primarily of the Buckingham type [for CeO_2,[10] ZrO_2,[11] and CaF_2.[12] For UO_2 we use the potential developed by Basak *et al.*,[13] comprised of a Buckingham term plus a Morse term, which has been shown to be one of the better potentials for describing UO_2, especially its defect properties.[14] The system sizes considered range from 1000 to 9000 atoms, depending on the

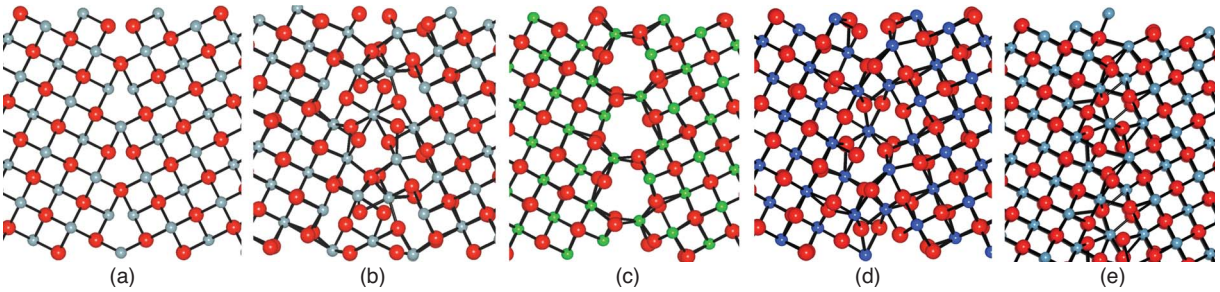

FIG. 1. (Color online) Structure of the $\Sigma5(310)/[001]$ symmetric tilt grain boundary: (a) idealized $\Sigma5$ tilt grain boundary, lowest energy structure found for (b) UO_2, (c) CeO_2, (d) ZrO_2, and (e) CaF_2. The light colored/small atoms are cations while the dark/larger atoms are anions.

thickness of the crystalline layers. The dimensions of the systems vary with chemistry due to the different lattice constants and the need to meet the minimum image convention (we use a potential cutoff of 0.8 nm). For UO_2, the dimensions within the boundary plane are 1.64×1.73 nm^2, for CeO_2 1.62×1.71 nm^2, for ZrO_2 2.04×1.61 nm^2, and for CaF_2 3.04×3.21 nm^2. The dimensions perpendicular to the grain-boundary plane vary from 2 to 22 nm, depending on the calculation (as will be discussed below). All calculations are performed at 0 K and at constant volume. However, select calculations were performed in which the pressure perpendicular to the grain-boundary plane was relaxed; the results of such calculations were qualitatively similar to those performed under constant volume.

To validate the effects seen with the empirical potentials, we use DFT. The DFT calculations of UO_2 use the projector augmented-wave method as implemented in the Vienna *ab initio* simulation package.[15] The exchange-correlation functional used is the spin-polarized, generalized gradient approximation with the Hubbard U correction (SP-GGA+U), with a U_{eff} (U-J) value of 3.96 eV;[16] the Hubbard U term is included to account for the effect of the strong correlation of $5f$ electrons in uranium. In the DFT calculations, we use a cell of 360 atoms for the structural optimization where the cell volume is kept constant and the atomic positions are relaxed. The Brillouin zone sampling is a $1\times1\times1$ Monkhorst-Pack k-point mesh;[17] the cut-off energy for the plane waves is 400 eV.

The structure of the $\Sigma5(310)/[001]$ symmetric tilt grain boundaries considered in this work are found by calculating the γ surface—the energy surface versus relative translation of the two grains—for each of the four materials. That is, once the ideal structure is generated using the online software GBSTUDIO,[18] the two microscopic degrees of freedom describing the relative translation between the two grains are minimized by mapping the energy of the system as a function of the relative translation between the two grains. We calculate the γ surface using a 5×10 grid of points for systems where the layer thickness is relatively small. We assume that the same boundary structure is the most stable structure for thicker layers. The lowest energy structure identified via this procedure is then used to study the electrostatic properties of the system. Since these interfaces are formed by joining two (310) surfaces of fluorite, which are charge neutral (type 1 in the notation of Tasker[19]), there is no inherent dipole created across these boundaries.

The electrostatic potential associated with a given ion is the measure of the Coulomb interaction per unit charge experienced by that ion. For the empirical-potential calculations, this is directly related to the energy of the system, being a sum of the products of the charge of each ion and the electrostatic potential at that ion's position. The electrostatic properties of each system are calculated using GULP.[20] In DFT, the average electrostatic potential for each ion is calculated by placing a test charge at each site and summing the Coulomb interaction between that test charge and all of the other charge in the system, both ionic and electronic.

III. RESULTS

To characterize the generality of the behavior we observe, we calculate the lowest energy $\Sigma5$ symmetric tilt boundary structure for the prototypical fluorite CaF_2 and three technologically important fluorite-structured materials: UO_2, CeO_2, and ZrO_2. (Strictly, ZrO_2 does not have the fluorite structure, but as yttria-stabilized ZrO_2 does have the fluorite structure, and the fluorite structure is reproduced by the potential being used, we will refer to ZrO_2 as fluorite structured in this paper). By mapping the γ surface for each material, we find the four structures illustrated in Fig. 1. Typically, the anion sublattice reconstructs much more than the cation sublattice upon minimization, forming ring structures around cations near the grain-boundary plane. The cation structures of the grain boundary in ZrO_2 and CaF_2 are very similar to one another and, as will be discussed below, similar to the experimentally determined structure for the $\Sigma5(310)/[001]$ tilt boundary in yttria-stabilized ZrO_2. The cation structure of the boundary in UO_2 is actually very similar to that of the ideal structure shown in Fig. 1(a). The cation structure of CeO_2 is altogether different, characterized by bridging bonds across the interface to anions. For each material, there are a number of local minima on the γ surface that span a large range of energy. For UO_2, the energy difference between the highest and lowest energy structures is 11 eV/nm^2 (1.76 J/m^2); for ZrO_2, 17.14 eV/nm^2; for CeO_2, 12.87 eV/nm^2; and for CaF_2, 4.45 eV/nm^2. As the simulated structure for each system is periodic in all three dimensions, there are two grain boundaries in each simulation cell, describing an infinite stacking of layers.

As shown in Fig. 2, each of these materials exhibits a complex electrostatic potential profile as a function of dis-

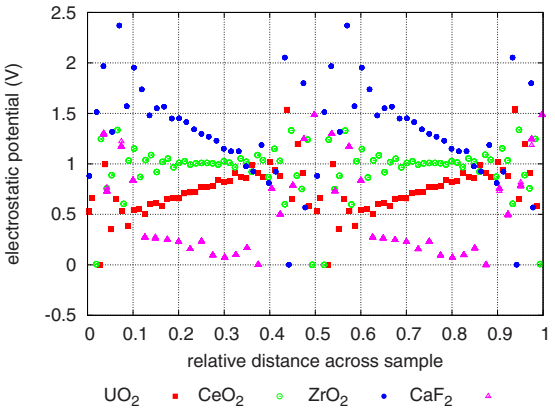

FIG. 2. (Color online) Electrostatic potential at the cation site for all the fluorite structures studied (UO_2, CeO_2, ZrO_2, and CaF_2) as a function of distance from the grain boundaries, scaled against the total length of the system for clarity. The thickness of the layers is 3.5, 3.4, 2.4, and 1.6 nm, respectively (these distances correspond to 1440 atoms for the first three materials and 2880 for CaF_2, which is larger because of the larger grain-boundary plane).

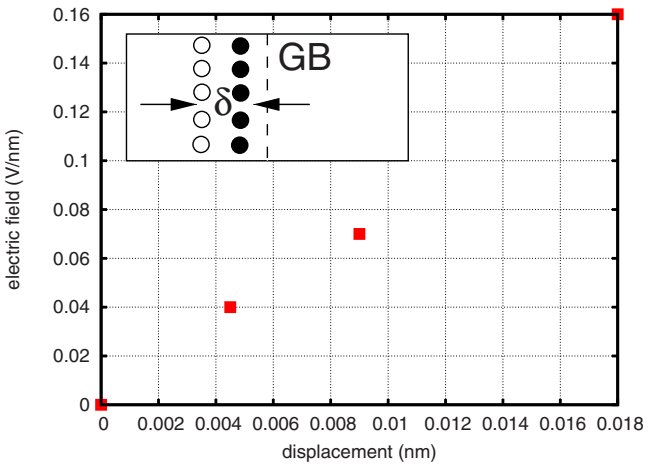

FIG. 3. (Color online) Electric field in a symmetrically-structured boundary as a function of the displacement δ of a plane of oxygen ions toward the boundary. The inset shows the direction and the plane of the displacement relative to the grain boundary (dashed line). The open symbols are the original oxygen positions, the filled circles are the final positions. The thickness of the layers is 10.4 nm in this calculation, corresponding to 2160 atoms.

tance across the boundaries and the layers themselves. While the details differ, there are similarities among the materials. Most prominently, the electrostatic potential in each system exhibits an abrupt change across the boundary, which we define as Φ_{GB}. The creation of Φ_{GB} across the boundary is similar to that described by Duffy and Tasker.[7] In the single-crystal regions, however, the electrostatic potential varies linearly, representing a constant electric field across each layer. As the two grain boundaries in the system are equivalent, the same electric field is established across each layer, compensating the discontinuity in electrostatic potential at each boundary. The change in electrostatic potential across the boundary is solely a function of the grain-boundary structure and is thus independent of the layer thickness. Φ_{GB} is considerably different for each of the materials. For ZrO_2, Φ_{GB} is relatively large, much more so than for UO_2. However, Φ_{GB} for CaF_2 is relatively small and essentially zero for CeO_2. These differences arise from the preferred atomic structure of the boundary, which is a function of the chemistry of each material.

In order to understand the origins of Φ_{GB}, we have examined alternative grain-boundary structures. As discussed, for each material there are multiple local minima on the γ surface of varying energy, each representing an atomically distinct $\Sigma 5$ grain-boundary structure. In the case of UO_2, the highest energy minimum on the γ surface exhibits no Φ_{GB}. Comparing this structure with the lowest energy structure, which does exhibit a finite Φ_{GB}, we find that the atomic structure of the higher energy grain boundary is mirror symmetric across the grain-boundary plane, while that of the lowest energy grain boundary exhibits a slight asymmetry arising from reconstruction. This asymmetric reconstruction is not related to the crystallographic asymmetry associated with grain boundaries in which the two grains have differing orientations. Moreover, it is not a direct consequence of the relative translation of the grains. Indeed, the symmetry of the system is preserved if the grains are only translated; it is upon atomic relaxation of the translated system that the symmetry is broken and Φ_{GB} is created across the boundary.

There is thus a relationship between the symmetry of the atomic structure at the grain boundary and the existence of Φ_{GB}. This conclusion is supported by calculations on the fully symmetric high-energy structure. As described above, this structure manifests no Φ_{GB}. However, Fig. 3 illustrates that an electric field corresponding to Φ_{GB} is generated as a plane of oxygen ions on one side of the $\Sigma 5$ boundary which is displaced slightly toward the boundary, with all of the other ion positions kept fixed. As the displacement δ increases, so does the electric field. Indeed, displacements of only 0.01 nm are sufficient to create fields similar in magnitude to those observed in the intermediate-layer thicknesses of 5 nm (compare this to the atomic displacements upon relaxation of the translated system, some of which are nearly 0.15 nm). Thus, while in the real grain-boundary structure the asymmetry is a complex distortion of the ionic positions rather than a simple displacement of a plane of ions, this result indicates that even crystallographically much simpler small distortions can lead to appreciable effects. A similar effect also occurs in a perfect crystal when a plane of atoms is displaced slightly. However, in that case, the system would relax back to the original geometry. In the case of the grain boundaries considered here, the displacements are an inherent part of the atomic structure of the boundary, thus leading to a permanent dipole within the material.

All of the calculations discussed above rely upon empirical potentials. To ensure that the observed effect is not an artifact of the simulation methodology, we have calculated the electrostatic potential for the smallest layer thickness (1.7 nm) in UO_2, shown in Fig. 4, using electronic-structure methods at the level of DFT. For this small layer thickness, it is more difficult to observe the profile in the electrostatic potential seen for the thicker layers in Fig. 2. Nevertheless, an abrupt change in the electrostatic potential across the

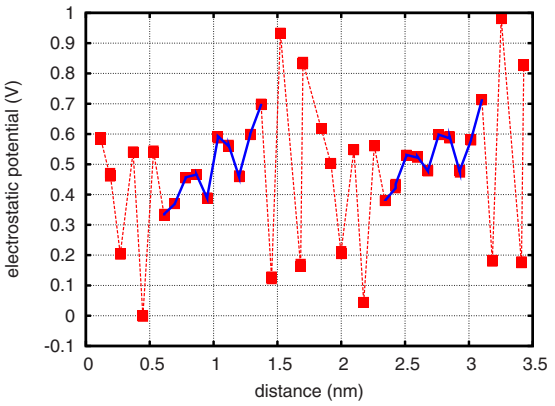

FIG. 4. (Color online) Electrostatic potential in UO_2 versus distance from the grain boundary as calculated with DFT. The lines are guides for the eyes—the dashed line is the electrostatic potential near the grain boundaries while the solid line is the potential within each crystalline layer.

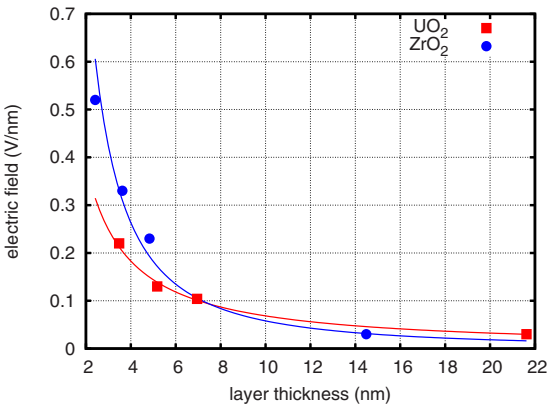

FIG. 5. (Color online) Electric field as a function of grain size for UO_2, CeO_2, and ZrO_2. The lines are guides for the eyes.

boundaries (dashed line) along with a roughly linear compensating potential within the crystalline layers (solid line) is clear, consistent with the empirical-potential calculations. The DFT structure is very similar to that found from the empirical potential; the atomic positions calculated with both methods are the same within 0.017 nm. Thus, DFT validates the observation from the empirical potentials that internal asymmetries can arise in these grain-boundary structures and that, when they do, a dipole is created that leads to Φ_{GB}. However, we note that DFT does find that the fully symmetric grain-boundary structure is lower in energy than the reconstructed asymmetric structure by 0.86 eV/nm^2.

As described above, the origin of the electric field in these nanostructured ceramics is a slight asymmetry in the atomic structure at the grain boundary. This asymmetry means that each grain boundary now has an orientation depending on the direction in which the symmetry is broken. We will refer to this orientation as the polarity of the grain boundary, in analogy with the properties of capacitors. In the stacked layer structures described above, the polarity of all of the grain boundaries is in the same direction, each with a given Φ_{GB}. In the case of an infinite stacking of layers with no external boundary conditions, this would lead to an infinite "staircase" of electrostatic potential. In our calculations, however, because of the periodic boundary conditions, we essentially impose the condition that, at the periodic boundary, the electrostatic potential is single valued, or, in other words, that the net change in electrostatic potential across the material is zero. Thus electrically, the system is short circuited. As a result, one end of the staircase is shifted down, resulting in the sawtooth potential we observe in Fig. 2. This is the origin of the electric field we observe within the crystalline layers. It should be noted that in a real material, a single grain boundary could have different spatial regions of differing polarities, which may lead to even more complex electrostatic effects.

The electric field we observe is thus a consequence of short-circuit electrical boundary conditions. Such electrical boundary conditions could be imposed in a real material by connecting both ends of the layered material to a conductor, which has a net potential change of zero across it. In fact, the potential profile within the ceramic could be continuously changed from a sawtooth to a staircase by controlling the potential change across the conductor. The boundary itself acts as a capacitor, with a constant electrostatic potential drop across it; the precise nature of the potential across each crystalline layer is a consequence of the type of electrical boundary conditions on the material. Thus, the system acts as a series of capacitors and dielectrics, formed on the nanoscale from a single-phase material.

We observe that, for each materials system, the electrostatic potential drop across the grain boundary is the same regardless of the thickness of the crystalline layers. That is, it is determined by the crystallography and atomic structure of the grain boundary alone. Since continuity forces the electrostatic potential increase across each layer to compensate the change across the boundary Φ_{GB}, the electric *field*, proportional to the potential change over the layer thickness, necessarily weakens as the layer thickness is increased. That is, the strength of the electric field is inversely proportional to the layer thickness of the material. Figure 5 shows this trend over a wide range of layer thickness and compares the trend between UO_2 and ZrO_2. For thin layers, ZrO_2 clearly has a stronger electric field than UO_2. As the thickness of the layers is increased, the field in ZrO_2 decreases more rapidly, such that at layer thicknesses of 20 nm UO_2 has the stronger field. This behavior is very sensitive to the structure of the grain boundary.

One can imagine that the polarity of a sequence of grain boundaries will depend on how the symmetry is broken at each boundary. If the sequence were of alternating polarity, then the condition of net zero-potential change, short-circuit electrical boundary conditions, would be automatically satisfied and no shifting of the potential would be necessary. This would lead to a square-wave pattern in the electrostatic potential. The open symbols in Fig. 6 shows the electrostatic potential in UO_2 for the case when the grain boundaries have alternating polarity [the case where the polarity is always in the same direction (closed symbols) is shown for comparison]. In this case, as each boundary has an equal but opposite change in electrostatic potential Φ_{GB}, the net polarity of the material is zero and no electric field is created within the

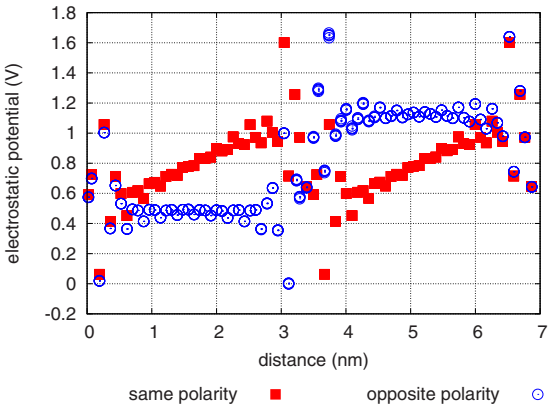

FIG. 6. (Color online) Electrostatic potential of nanolayered UO_2 in which the grain boundaries have the same polarity (red/square symbols) and opposite polarity (blue/circle symbols). See text for definition of polarity.

single-crystalline layers of the material. However, the layers do support constant electrostatic potentials of different magnitude. The energy difference between the two boundary structures is only 0.06 eV/nm^2 per grain boundary, with the opposite polarity structure being of higher energy.

By changing the sequence of polarity of the grain boundaries and imposing specific electrostatic boundary conditions, the electrostatic properties of the material could be controlled to a very high degree, as shown schematically in Fig. 7. If the net polarity of the material were zero (i.e., there were equal numbers of each polarity), the electrostatic-potential profile would not depend on the external boundary conditions and regions of high and low electrostatic potential would be established. If, on the other hand, there were a net polarity to the material and the material were subjected to short-circuit electrostatic boundary conditions, electric fields would be created across the layers. In reality, controlling the polarity sequence would likely be very challenging experimentally.

IV. DISCUSSION

The controllable polarity of the grain boundaries and the possibilities of a bulk electric field in nanolayered ceramics have profound consequences. For instance, when an electric field is created, this field will strongly modify the behavior of charged defects. For example, impurities and fission products

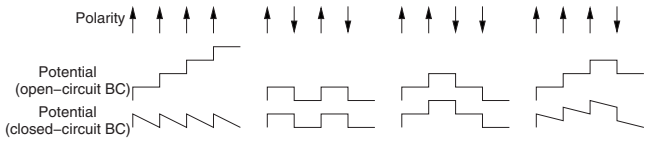

FIG. 7. Electrostatic potential as a function of both the polarity sequence of the grain boundaries and the electrical boundary conditions across the material. If the sequence contains equal numbers of each polarity, the two profiles are identical. However, if there is more of one polarity than the other, if short-circuit boundary conditions are applied, an electric field will be established across the layers.

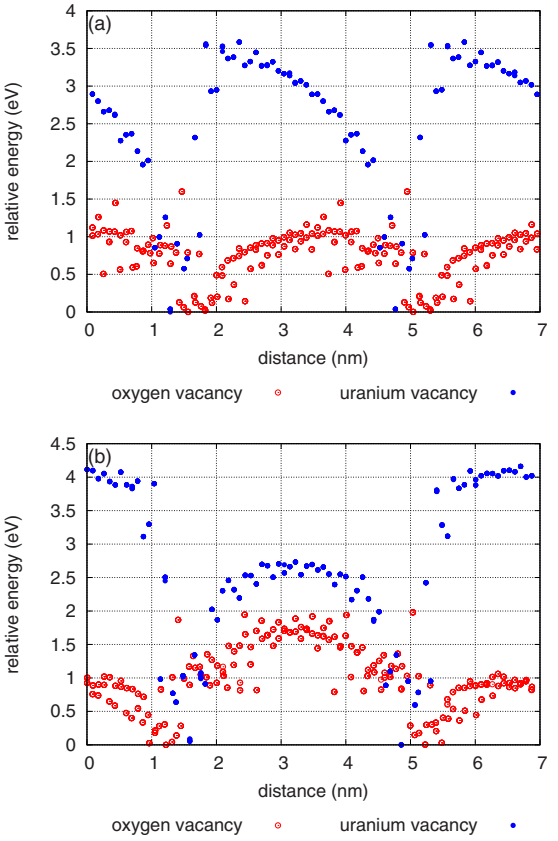

FIG. 8. (Color online) Energy of oxygen and uranium vacancies relative to the lowest energy site in nanolayered UO_2 where (a) the two grain boundaries have the same polarity and (b) the two grain boundaries have alternating polarity.

in UO_2 can have a net charge relative to the host lattice that will interact with the electric field. This means that segregation effects will be greater in the presence of the electric field than in its absence. Furthermore, the interaction range between the grain boundaries and the defects will span the entire thickness of the layer. Thus, while the electric field decreases with layer thickness, defect-boundary interactions will still be very long ranged. Even in materials where there is no electric field because the net polarity of material is zero, there will be a natural segregation of positively versus negatively dopants to different layers. This offers the potential for very fine control of dopant segregation profiles, for example.

These effects are illustrated in Fig. 8 for the oxygen and uranium vacancies for systems in which the grain-boundary polarity is the same [Fig. 8(a)] and alternates [Fig. 8(b)]. Relative to the host lattice, the oxygen vacancy has a positive charge ($+1.2e$ and $-2.4e$, respectively, within the Basak potential). Thus, each defect would be expected to interact in opposite ways with any electrostatic potential. Indeed, in both cases, the uranium vacancy behavior is essentially the opposite of that of the oxygen vacancy. In the case of aligned polarity, the generated electric field pushes the two types of defects in opposite directions, to opposing sides of each grain. If, for example, defects were generated within one grain via a collision cascade, positive defects would be pushed to one boundary and negative defects to the other. In the case of

alternating polarity [Fig. 8(b)], there is no field to push the defects. However, as discussed above, positive defects prefer one layer and negative defects another. There is thus a natural segregation of different types of defects. Charged dopants and impurities would be expected to behave in a very similar manner. Further, the difference in segregation tendency due to the electrostatic potential is also illustrated in Fig. 8, which indicates that the defect with the greater charge (the uranium vacancy) is influenced to a greater extent than the lesser-charged oxygen vacancy. This may lead to the creation of a space charge that would create new electrostatic effects that may enhance or negate the inherent electrostatic potential of the grain boundary.

The electric field described here is fundamentally different from that caused by space charge. Space charge is conventionally viewed as a build up of charge at an interface due to differing tendencies of different types of defects to segregate to the interface. For example, if interstitials of one species segregate to the interface in greater numbers than those of another species (e.g., O vs U), then the stoichiometry of the material near the interface is different than the bulk and a build up of charge occurs, resulting in an electric field. However, this build up of charge is the result of thermal segregation of defects to the boundary and as such is a finite-temperature effect. The electric potential described in this work is an intrinsic zero-temperature effect, one that exists as a direct consequence of the atomic structure of the boundary, not because of defect segregation to the boundary.

It is useful to compare and contrast the effect seen here with that observed by Duffy and Tasker.[7] They also saw a potential drop across a grain boundary. However, the origin of that potential drop is different. They specifically examined boundaries that were created from two polar surfaces. When the spacing between atomic planes at the boundary is different than in the crystalline layers, a dipole is created at the boundary, resulting in the potential drop. Thus, the effect they describe is the direct consequence of creating boundaries from polar surfaces. In the case of NiO, they found a dilation—an increase in the planar spacing at the boundary—of nearly 0.1 nm. The dipole is therefore created from a combination of this dilation and an asymmetry in the arrangement of the ions: anions exist on one side of the boundary and cations on the other. In our case, we find a potential drop even in boundaries created from neutral (310) surfaces, due to an asymmetry in the atomic structure, not the ionic arrangement, resulting from atomic distortions of about 0.01 nm. Thus, while the net effect is the same—a drop in potential across the boundary—our results suggest that it is much more general and should occur in a much wider range of boundary types.

Above, we validated our empirical potential results by comparing with DFT. Further validation is given by comparing to experimental observation of the structure of grain boundaries in these materials. While high-resolution results are not available for UO_2, CeO_2, or CaF_2, there are such experiments for ZrO_2. In particular, Dickey *et al.*[9] performed Z-contrast scanning transmission electron microscopy (Z-STEM) on $\Sigma 5(310)$ grain boundaries in yttria-stabilized ZrO_2 and found a cation structure that was subsequently reproduced via DFT calculations[21] (note that the experiments did not resolve the anion structure of the boundary). The structure involves two rows of Zr ions on each side of the boundary merging to form one column, forming a structure very similar to that found via the empirical potential in the current work, as illustrated in Fig. 9. Thus, the two approaches result in cation structures very similar to the experimentally observed structure. The two theoretical approaches do predict very different anion structures and identifying the anion structure experimentally could distinguish between the two. The empirical potential used only mimics yttria-stabilized ZrO_2 and does not explicitly account for the Y ions. Any electrostatic potential generated within the material would lead to a segregation of Y ions, potentially modifying the strength of the potential. Thus, our results should be regarded as indicating a general physical trend, not an absolute quantitative prediction of the size of the electrostatic effects.

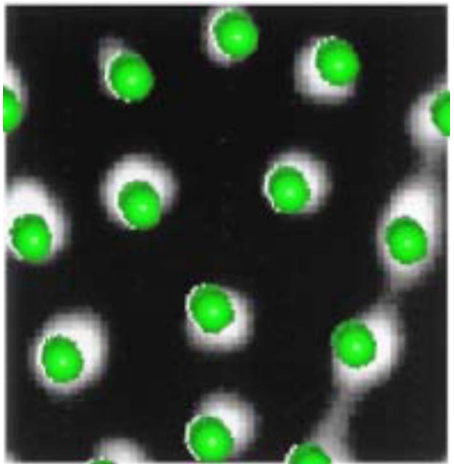

FIG. 9. (Color online) Cation structure of a $\Sigma 5(310)$ tilt grain boundary in ZrO_2 as found by Dickey *et al.* (Ref. 9) (Z-STEM image) and the cation structure found from the current calculations (spheres).

V. CONCLUSION

To conclude, we have found that grain boundaries in ceramics can reconstruct to break symmetry. The origins of this symmetry breaking are different than that observed by Duffy and Tasker. In their case, the boundaries were created from non-neutral surfaces and the potential drop formed at the grain boundary was from a larger separation of atomic planes at the boundary than in the crystalline layers. Here, the potential drop occurs at boundaries created from nonpolar interfaces due to very small distortions (about 0.01 nm) of the atomic positions. Thus, the effect they first described is much more general than originally envisaged and can occur in a much wider range of boundary types. In fact, our results are similar to the effects Duffy describes for asymmetric grain boundaries.[8] The net result in both cases is similar: a change in electrostatic potential as the boundary is crossed. We have found that the magnitude of this electrostatic effect is very sensitive to the chemistry of the material. Strong effects are produced in UO_2 and a system meant to mimic yttria-

stabilized ZrO_2, but is relatively weak or nonexistent in CeO_2 and CaF_2. We have also seen how controlling the polarity of the boundary can lead to complex profiles of electrostatic potential that greatly modify defect behavior and could be used to control defect and dopant segregation in multilayered ceramics. Furthermore, electric fields can be established in these layers and could be realized in experiments by short circuiting the multilayer stack with a conductor. As multilayered ceramics with nanometer length scales can now be synthesized via methods such as pulsed laser deposition,[22] opportunities exist for exploring this effect. To the extent that the electrostatic potential within the crystalline layers can be controlled, or at least exploited, by controlling the grain-boundary structure, these results may lead to new possibilities for engineering nanostructured ceramics.

ACKNOWLEDGMENTS

Work at LANL was sponsored by the U.S. Department of Energy, Office of Basic Energy Sciences, Division of Materials Science and Engineering. P.V.N. also acknowledges support from the Seaborg Institute at LANL. Los Alamos National Laboratory is operated by Los Alamos National Security, LLC, for the National Nuclear Security Administration of the U.S. Department of Energy under Contract No. DE-AC52-06NA25396. S.B.S. and S.R.P. gratefully acknowledge support from the National Science Foundation through Grant No. DMR-0426870. C.R.S. and P.N. gratefully acknowledge support from the Nuclear Energy Advanced Modeling and Simulation (NEAMS) program. The authors also wish to thank Cetin Unal for informative discusions.

*Corresponding author; blas@lanl.gov

[1] A. Misra, M. J. Demkowicz, X. Zhang, and R. G. Hoagland, J. Miner. Met. Mater. Soc. **59**, 62 (2007).
[2] Y. T. Zhu and X. Liao, Nature Mater. **3**, 351 (2004).
[3] H. Zheng, J. Wang, S. E. Lofland, Z. Ma, L. Mohaddes-Ardabili, T. Zhao, L. Salamanca-Riba, S. R. Shinde, S. B. Ogale, F. Bai, D. Viehland, Y. Jia, D. G. Schlom, M. Wuttig, A. Roytburd, and R. Ramesh, Science **303**, 661 (2004).
[4] J. Frenkel, *Kinetic Theory of Liquids* (Oxford University Press, New York, 1946).
[5] K. Lehovec, J. Chem. Phys. **21**, 1123 (1953).
[6] K. L. Kliewer and J. S. Koehler, Phys. Rev. **140**, A1226 (1965).
[7] D. M. Duffy and P. W. Tasker, J. Appl. Phys. **56**, 971 (1984).
[8] D. M. Duffy, J. Phys. C: Solid State Physics **19**, 4393 (1986).
[9] E. C. Dickey, X. D. Fan, and S. J. Pennycook, J. Am. Ceram. Soc. **84**, 1361 (2001).
[10] S. Vyas, R. W. Grimes, D. H. Gay, and A. L. Rohl, J. Chem. Soc., Faraday Trans. **94**, 427 (1998).
[11] M. O. Zacate, L. Minervini, D. J. Bradfield, R. W. Grimes, and K. E. Sickafus, Solid State Ionics **128**, 243 (2000).
[12] S. Vyas, R. W. Grimes, V. L. Bulatov, and M. Abramowski, Mol. Simul. **26**, 307 (2001).
[13] C. B. Basak, A. K. Sengupta, and H. S. Kamath, J. Alloys Compd. **360**, 210 (2003).
[14] K. Govers, S. Lemehov, M. Hou, and M. Verwerft, J. Nucl. Mater. **366**, 161 (2007).
[15] G. Kresse and J. Furthmüller, Phys. Rev. B **54**, 11169 (1996).
[16] P. Nerikar, T. Watanabe, J. Tulenko, S. R. Phillpott, and S. B. Sinnott, J. Nucl. Mater. **384**, 61 (2009).
[17] H. J. Monkhorst and J. D. Pack, Phys. Rev. B **13**, 5188 (1976).
[18] H. Ogawa, Mater. Trans. **47**, 2706 (2006).
[19] P. W. Tasker, J. Phys. C **12**, 4977 (1979).
[20] J. Gale, J. Chem. Soc., Faraday Trans. **93**, 629 (1997).
[21] Z. Mao, S. B. Sinnott, and E. C. Dickey, J. Am. Ceram. Soc. **85**, 1594 (2002).
[22] D. B. Chrisey and G. K. Hubler, *Pulsed Laser Deposition of Thin Films* (Wiley, New York, 1994).